Single-Molecule LEDs from Nanoscale Electroluminescent Junctions†

Tae-Hee Lee and Robert M. Dickson*

School of Chemistry and Biochemistry, Georgia Institute of Technology, Atlanta, Georgia 30332-0400

Received: January 5, 2003; In Final Form: March 15, 2003

Through pulsed operation, polarity is introduced in single Ag nanocluster (Ag_2-Ag_8) electroluminescence within seemingly nonpolar two-terminal nanoscale break junctions at room temperature. While observable with much higher power DC excitation, both high-frequency pulsed and AC operation lead to greatly increased spectrally and thermally stable electroluminescence with much narrower individual nanocluster electroluminescence spectra. Being polarity independent under both sinusoidal and DC excitations, pulsed electrical excitation of individual Ag nanoclusters has generated the first single-molecule LED by temporally separating hole and electron injection processes.

Introduction

As device dimensions continue to shrink, nanoscale electronics will eventually rely on true molecular-scale junctions.[1,2] Unfortunately, while complicated fabrication and characterization methods have been employed, such nanoscale devices rarely show strong polarity dependence in charge transport.[3−10] Much of the problem in observing polarity in nanoscale electronic devices results from the difficulty of fabricating nanoscale heterojunctions.[11,12] In bulk, macroscopic heterojunction structures yield clear diode behavior and many materials can be made to electroluminesce with polarity-dependent device architectures. Even in the most advantageous nanoscale devices, however, experiments are performed only with DC voltages for ease of measurement and avoidance of frequency-dependent material response. Consequently, the frequency response is largely ignored. Utilizing novel two-pulse excitation to control charge transport through a nanoscale junction, we have created a light-emitting diode (LED) junction made of many spatially isolated individual silver nanoclusters (Ag_2-Ag_8) readily formed between semiconducting silver oxide electrodes.[13] Highly thermally and spectrally stable under AC excitation, charge transport, and emission appear to be polarity independent under both DC and AC excitations. When charge injection processes under pulsed excitation are separated, however, single-molecule LED operation is readily achieved in seemingly symmetric devices.

Experimental Section

Three different film deposition methods were used to prepare slightly oxidized silver thin films for our study.[13] All three methods—thermal evaporation, chemical bath deposition, and RF sputtering—give 15−80-nm thick films that all yield similar results. After deposition on glass cover slips, thin silver films are activated with DC current to form nanoscale junctions composed of a single line of silver nanoclusters surrounded by a micronscale optically distinguishable region on either side. While the Ag nanoclusters have similar optical properties to those prepared in solution,[14−16] this dry, surface-bound, Ag nanocluster-containing nanoscale break junction is gently formed by not exceeding 3 V of constant DC voltage in the current-limited fabrication.[13,17] From <500-Ω initial film resistance with typical film dimensions of 50 nm × 100 μm × 200 μm, the continuous films exhibit slowly increasing conductivity with continued applied voltage. After less than a minute of slowly increasing conductivity during further activation, a sudden conductivity increase is followed by an abrupt increase in resistance to $>10^6$ Ω as the junction forms through electromigration.[17,18] The activation charge consumption primarily depends on the cross section of the activation area but typically consumes ~0.1 C/μm^2. While the silver-rich junction is surrounded by a silver oxide area spanning at most 5 μm, the remaining film area is reduced to metallic silver as evidenced by the electrical conductivity and elemental quantification with electron dispersive spectroscopy.[19]

Detailed experimental procedures are as previously described,[13,19] therefore, only a brief experimental description is presented here. Electrical excitation is performed through computer controlled DC (Agilent E3646A), high-frequency sinusoidal AC (70−300 MHz, MiniCircuits ZOS-150 and ZOS-300) or pulsed excitation. High-frequency, narrow electrical pulses from two independent channels (Datron 2000, 1−200-MHz repetition rate, and 2-ns minimum pulse widths) are combined in a high-frequency combiner (MiniCircuits ZSC-2-1) and applied to the samples through high-frequency, low-loss SMA cables designed for radio frequency applications. Samples were generally kept under 10^{-5}-Torr vacuum during operation to reduce oxidation of the electroluminescent nanoclusters and greatly extend device lifetime. Ag nanocluster electroluminescence is collected through an Olympus IX70 inverted microscope equipped with a 1.4-NA, 100× U-plan apo objective and imaged with a high-sensitivity CCD camera (Roper Scientific). Emission intensity of all electroluminescent nanoclusters is correlated with excitation conditions (e.g.. voltage, frequency/repetition rate, and pulse parameters in the composite two-pulse waveform). Individual nanocluster electroluminescence spectra are collected through a 300-mm imaging monochromator (Acton Research Corp.) equipped with either a mirror for direct imaging of the individual features or a 150 l/mm grating to record their emission spectra.

† Part of the special issue "Arnim Henglein Festschrift".

* To whom correspondence should be addressed. E-mail: dickson@chemistry.gatech.edu.

10.1021/jp034020+ CCC: $25.00
Published on Web 04/24/2003

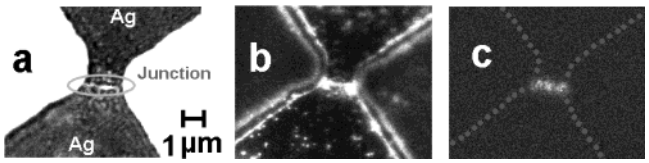

Figure 1. Microscopic images of a typical silver nanocluster break junction formed by electromigration. The nanoscale break junctions were prepared on photolithographically etched RF sputtered thin silver films. Images were collected on a high-sensitivity monochrome CCD camera (MicroMax, Roper Scientific) through a 1.4 numerical aperture 100× plan apochromat oil immersion objective (Olympus) with 1.5× magnifier. (a) Transmitted light image of the electrodes and junction. (b) Fluorescence (>525 nm) from the line of individual silver nanoclusters within the junction under filtered mercury arc lamp excitation (450−480 nm). Fluorescence from photoactivated silver nanoclusters is also observed several microns away from the junction and along the electrode edges. (c) Electroluminescence from individual silver nanoclusters within the same junction as in (a) and (b) under ±2.5 V sinusoidal excitation at 160 MHz. Electrode edges are indicated with gray dots. Only nanoclusters within the junction electroluminesce.

Results and Discussion

With applied DC electric fields in evacuated ambient conditions (10^{-5} Torr), the array of individual nanoclusters electroluminesces with an intensity that is proportional to the current.[13] The electroluminescence[13,19] (EL) shows similar emission behavior to that of photoactivated silver nanoclusters[20,21] with multicolored single dipolar emission patterns and blinking. Both of these emission characteristics indicate the EL is from single nanoclusters formed within the nanoscale break junction and is distinct from recent reports of plasmon emission from thin metal films.[22,23] The line of EL features also clearly fluoresces under mercury lamp excitation (Figure 1). While fluorescent Ag_n can be photochemically produced on the oxide electrodes near the junction, the electrodes transporting current to the nanocluster junction remain continuous and, therefore, highly conductive, such that holes and electrons only recombine at the line of nanoclusters within the break junction. This extremely narrow recombination zone yields greatly enhanced EL intensity with low-voltage, high-frequency AC excitation (typically ranging from 150−170 MHz) by injecting charge at precisely the optimal time. The resonant frequency of the junction arising from the combination of resistance, inductance, and capacitance within this circuit (an RLC circuit) is determined by the apparently symmetric oxide−oxide homojunction structure, thereby setting the characteristic time response of the junction at ∼6.25 ns. This behavior corresponds to a series RLC circuit with $R = 45\ \Omega$, $L = 0.48\ \mu$H, and $C = 2.1$ pF for the EL process. Inductance L in such high-frequency nanodevice responses has been proposed to arise from the inertia of electrons in the >100-MHz frequency range.[24] This resonant AC excitation not only greatly extends device lifetimes by minimizing thermal decay but also yields much longer lasting electroluminescent features exhibiting narrow emission spectra that are devoid of the broad and wide-ranging spectral dynamics characteristic of nanoclusters under comparable DC excitation (Figure 2).

The EL from and current through the junction are independent of DC polarity, suggesting homojunction behavior. This observed lack of polarity dependence in DC results from electron and hole injection processes not being separate. Because the Ag_n nanocluster HOMOs lie within the Ag_2O electrode band gap,[19] hole injection occurs through field dependent extraction of electrons which tunnel through the oxide layer: a symmetric process depending only on the potential difference. This field dependent hole injection into silver nanoclusters is then followed by electron reinjection from the anode and subsequent radiative

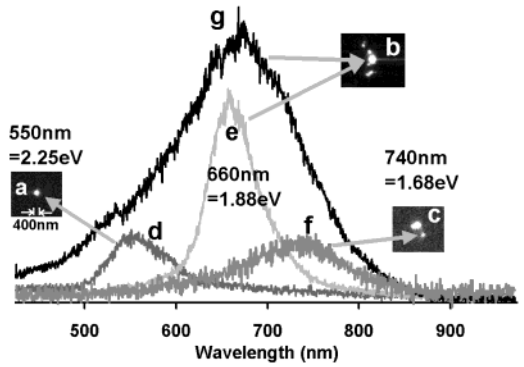

Figure 2. AC- and DC-excited single-molecule electroluminescence spectra. Emission from spatially resolved individual molecules was imaged through a 300-mm imaging monochromator (Acton) with a mirror in place of the grating. Slit width, position, and CCD region of interest were adjusted such that, upon rotating a 150 l/mm grating into the path, single-molecule spectra are readily obtained. Integration time for each spectrum is 15 s. Single-molecule images (a, b, and c) have corresponding AC-excited (160 MHz, ±2 V, and ∼100 nA) electroluminescence spectra d, e, and f, respectively, with emission maxima at 550, 660, and 740 nm. All AC-excited spectra are very stable. Spectrum f is magnified (3×) so that the peak can be clearly seen. The same nanocluster that yields spectrum e under AC excitation yields spectrum g under 7-V DC (∼1 mA) excitation, the voltage (and current) necessary to yield comparable EL intensity. While highly dynamic at short times, the DC spectral shape remains constant with integration time from 1.5 to 15 s as it averages over all emissive nanocluster sizes created under DC excitation. Clearly, DC-excited emission is much broader due to fast spectral dynamics resulting from severe chemical changes in the nanocluster which end up destroying it after several minutes. The 400-nm scale bar in (a) shows that individual emitters yield diffraction-limited images

recombination. The anode has a better electrical connection with the nanocluster resulting from the asymmetric DC junction fabrication which preferentially creates the nanoclusters closer to the anode.[18] Therefore, the nanocluster LUMO and the Ag_2O conduction band levels will have good overlap at the electrode operating as the anode in the junction fabrication. Throughout the text the anode is defined by the original DC nanoscale break junction fabrication. Crucial to the EL process, the oxide region surrounding the formed nanoclusters simultaneously acts as a barrier for the direct electron reinjection into the nanocluster ground states thereby enabling charge separation at the nanoclusters.[25−28]

To probe each step of the EL mechanism and introduce polarity, we separate the symmetric hole injection and asymmetric electron reinjection by applying two consecutive short electrical pulses at a repetition frequency much lower than the enhancement frequency. Polarities, widths, and interpulse delays of two consecutive pulses were controlled to examine the polarity dependence and time scales for each step of the EL process: hole injection, hole lifetime, and electron reinjection. With computer-controlled polarities, widths, and interpulse delay, two consecutive 2.5-V_{pp} electrical pulses at 33 or 40 MHz were combined into one composite waveform through a high-frequency pulse combiner, and the combined pulse train was then fed into the junction. Contrary to DC, pulsed excitation through the anode shows very strong polarity dependence, in which only positive followed by negative pulses give any detectable EL. Demonstrating the introduction of polarity in charge transport through the junction by separating each step of the process with short pulses, no other possible combination of two pulse polarities yields detectable emission (Figure 3a). While the field necessary for electron extraction is established

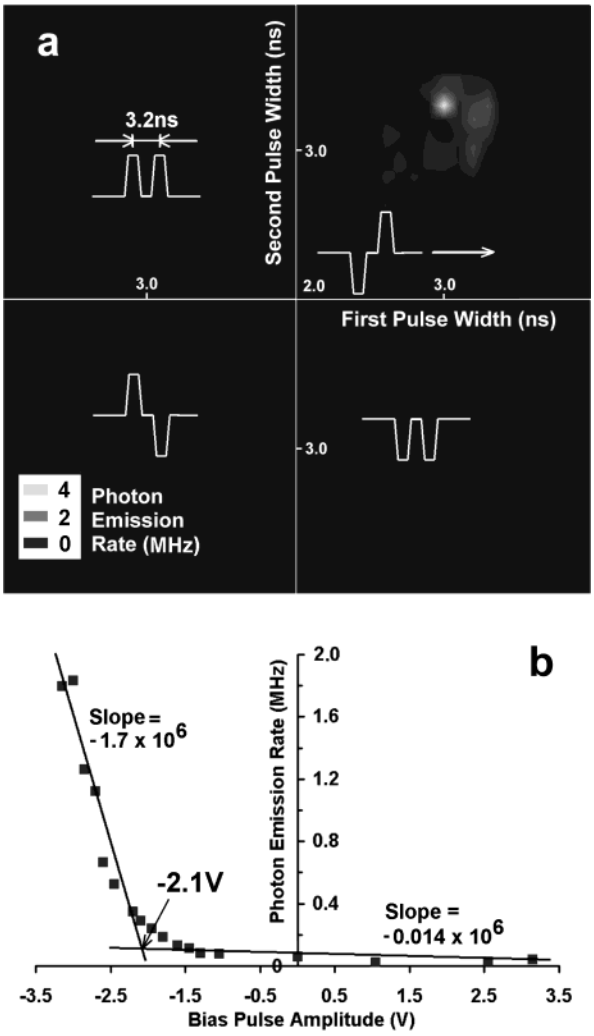

Figure 3. Total, detection efficiency corrected, EL intensity from the entire array of individual nanoclusters under various two pulse excitations. (a) EL intensity vs first and second-pulse widths and polarities (both pulses were of 2.5-V amplitude with 3.2-ns interpulse delay at 33-MHz repetition rate). The 3.2-ns interpulse delay was chosen because it gives the highest EL intensity. When applied to the anode, only positive pulses followed by negative pulses give detectable emission out of all possible pulse widths, polarities, and interpulse delays. The brightest emission was seen with a 3.0-ns first pulse, a 3.3-ns second pulse, and a 3.2-ns interpulse delay. (b) EL intensity from the entire junction vs second-pulse amplitude with 2.5-V positive first pulse at 40 MHz repetition rate. Pulse widths and interpulse delay were 2.8 and 4.0 ns, respectively. With increasingly negative second-pulse (bias pulse) amplitude, the EL response from the entire nanocluster array in the junction shows LED behavior with a −2.1-V threshold voltage. A change in slope of more than 2 orders of magnitude occurs at the threshold voltage. While individual molecules clearly saturate, the pulse pair voltages at which each saturates depends on its immediate nanoenvironment within the highly heterogeneous nanoscale junction. Consequently, overall device saturation and destruction occur at similar second-pulse voltages that are higher than those presented here. The voltage range presented in this figure is thereby unaffected by either saturation or thermal destruction.

by the first pulse, independent of polarity, the polarity requirements of the second-pulse yield the high-frequency asymmetry in the electroluminescence. If both processes are performed simultaneously, as in DC, no polarity is observed. Pulsed excitation, however, enables the first pulse to establish the field necessary to extract an electron and essentially charge the nanocluster region, which then acts as a charged capacitor. The polarity dependence is introduced only in the second pulse as it interacts with the charged junction and the asymmetric distribution of nanoclusters with energy levels more closely tied to those of the anode.[29] A second pulse of the same polarity cannot efficiently travel to the nanocluster region because of the junction capacitance and is incapable of producing EL. On the other hand, when the second-pulse polarity differs from that of the first, the traveling pulse passes through the nanocluster region and can directly interact with the individual Ag_n nanoclusters. Thus, to inject electrons into individual nanocluster excited energy levels to yield radiative recombination, the second pulse must be negative enough to reach the anodic silver oxide conduction band edge. Therefore, negative followed by positive pulses cannot produce nanocluster EL when applied to the anode. However, when the electrodes are swapped and pulses are applied to the cathode, this complementary polarity dependence (i.e., negative followed by positive pulses) is then the only pair observed to yield EL. Thus, electron injection occurs only with the second pulse through the anode being negative, due to its better electrical connection to the electroluminescent nanoclusters. Consequently, for either electrode configuration, polarity is observed in the electroluminescence from a seemingly nonpolar (i.e., DC, or sinusoidally, excited) device (Figure 3a).

Electroluminescence strongly depends on individual pulse and interpulse parameters. When pulses are applied to the anode, the strongest emission is observed with a ∼3.0-ns width positive first pulse (hole injection time) followed by a ∼3.3-ns negative second-pulse width (electron reinjection time) with an interpulse delay (hole lifetime) of at least 3.2 ns. The recombination lifetime was measured with a single-photon counting system to be ≪1.0 ns, which is far shorter than the 33-MHz repetition rate (30 ns), thereby avoiding saturation effects in the overall charge transport dynamics. The most efficient delay between two consecutive pulses is determined by the junction RLC resonance but suggests that the hole lifetime is at least 3.2 ns. The pulse widths giving maximum EL correspond to the specific AC enhancement frequency (∼160 MHz) of each sample, but at a lower repetition rate. This indicates that the high-frequency sample response dictates the optimal charge injection time scales for each step as well as the optimal period (6.25 ns with 160-MHz sinusoidal excitation) of the entire EL process. Experimentally, 160-MHz sinusoidal excitation is the best compromise to access all individual optimal EL time scales while still being much longer than the charge recombination lifetime measured with the single-photon counting system (<1 ns). This frequency optimally accesses the time necessary for charging the junction and injecting holes (shorter than the positive pulse width, 3.0 ns), the hole lifetime (longer than the interpulse delay, <3.2 ns), and the electron reinjection time (shorter than the negative pulse width, 3.3 ns).

Being polarity independent under DC operation, this apparent homojunction can yield bulk LED behavior when operated with short pulse pairs (Figure 3b). Simultaneously exciting all nanoclusters in the one-dimensional (1-D) nanoscale junction, out of the four possible polarity combinations with two consecutive pulses ranging in width from 2.5−3.5 ns, only positive pulses followed by negative pulses applied to the anode produce emission. Thus, provided that a ∼3-ns +2.5-V pulse is always added prior to the bias pulse (2.5−3.5 ns in width), diode behavior is observed with respect to the bias pulse as the nanocluster junction operates as an LED for the next ∼4 ns after the first pulse is applied. To examine the diode characteristics of the junction toward bias pulses, EL intensity was recorded with fixed +2.5-V 2.8-ns first pulses followed by 2.8-

ns second pulses with variable amplitude and fixed interpulse delay (4.0 ns). As shown in Figure 3b, only negative bias pulses (second pulses) more energetic than the threshold can get through the excited state molecular energy levels of silver nanoclusters while positive second pulses cannot produce emission in this electrode configuration, explicitly yielding high-frequency LED behavior from the array of Ag nanoclusters along the junction. Since this high-frequency polarity dependence is based on general physical processes and properties of materials, such as charging, capacitance, and discrete energy levels, it may be generally applicable to other molecular junctions if pulsed operation is not limited by materials and properly designed electrodes are used to trap and stabilize charges formed between pulses. Such is the case at nanoscale break junctions often used in DC molecular electronics studies.[3−10] Thus, similar pulsed methods are likely to reveal polarity in other seemingly symmetric two-terminal molecular electronics devices.

Arising from favorable energies within electrically written Ag_n nanocluster EL devices, polarity dependence of electroluminescence is introduced by using short enough pulses to separate each step of the process: electron extraction and reinjection. This step by step operation has enabled operation of this system as a 1-D array of high-frequency single-molecule LEDs and yielded detailed information about charge transport dynamics.[30] Utilizing the properties of robust metal nanoclusters[31] formed into an extremely narrow recombination zone which does not limit high-frequency excitation,[32] this high-frequency polarity dependence on the charge transport through a nanoscale junction may be of great help in building useful molecular electronic/optoelectronic devices.[12,33,34]

Acknowledgment. The authors gratefully acknowledge support from NSF CHE-9984507, the Dreyfus and Sloan Foundations and the Blanchard endowment for Junior Faculty.

References and Notes

(1) Aviram, A.; Ratner, M. A. *Chem. Phys. Lett.* **1974**, *29*, 277.
(2) Alivisatos, A. P.; Barbara, P. F.; Castleman, A. W.; Chang, J.; Dixon, D. A.; Klein, M. L.; McLendon, G. L.; Miller, J. S.; Ratner, M. A.; Rossky, P. J.; Stupp, S. I.; Thompson, M. E. *Adv. Mater.* **1998**, *10*, 1297.
(3) Klein, D. L.; McEuen, P. L.; Katari, J. E. B.; Roth, R.; Alivisatos, A. P. *Appl. Phys. Lett.* **1996**, *68*, 2574.
(4) Reed, M. A.; Zhou, C.; Muller, C. J.; Brugin, T. P.; Tour, J. M. *Science* **1997**, *278*, 252.
(5) Kagan, C. R.; Mitzi, D. B.; Dimitrakopoulos, C. D. *Science* **1999**, *286*, 945.
(6) Venkataraman, L.; Lieber, C. M. *Phys. Rev. Lett.* **1999**, *83*, 5334.
(7) Rochefort, A.; Ventra, M. D.; Avouris, P. *Appl. Phys. Lett.* **2001**, *78*, 2521.
(8) Park, J.; Pasupathy, A. N.; Goldsmith, J. I.; Chang, C.; Yaish, Y.; Petta, J. R.; Rinkoski, M.; Sethna, J. P.; Abruña, H. D.; McEuen, P. L.; Ralph, D. C. *Nature* **2002**, *417*, 722.
(9) Zhitenev, N. B.; Meng, H.; Bao, Z. *Phys. Rev. Lett.* **2002**, *88*, 226801.
(10) Reichert, J.; Ochs, R.; Beckmann, D.; Weber, H. B.; Mayor, M.; Löhneyse, H. v. *Phys. Rev. Lett.* **2002**, *88*, 176804.
(11) Duan, X. F.; Huang, Y.; Cui, Y.; Wang, J. F.; Lieber, C. M. *Nature* **2001**, *409*, 66.
(12) Yuan, Z.; Kardynal, B. E.; Stevenson, R. M.; Shields, A. J.; Lobo, C. J.; Cooper, K.; Beattie, N. S.; Ritchie, D. A.; Pepper, M. *Science* **2002**, *295*, 102.
(13) Lee, T.-H.; Gonzalez, J. I.; Dickson, R. M. *Proc. Natl. Acad. Sci. U.S.A.* **2002**, *99*, 10272.
(14) Ershov, B. G.; Janata, E.; Henglein, A. *J. Phys. Chem.* **1993**, *97*, 339.
(15) Ershov, B. G.; Janata, E.; Henglein, A.; Fojtik, A. *J. Phys. Chem.* **1993**, *97*, 4589.
(16) Zheng, J.; Dickson, R. M. *J. Am. Chem. Soc.* **2002**, *124*, 13982.
(17) Park, H.; Lim, A. K. L.; Alivisatos, A. P.; Park, J.; McEuen, P. L. *Appl. Phys. Lett.* **1999**, *75*, 301.
(18) Schimschak, M.; Krug, J. *Phys. Rev. Lett.* **1998**, *80*, 1674.
(19) Lee, T.-H.; Dickson, R. M. *Proc. Natl. Acad. Sci. U.S.A.* **2003**, *100*, 3043.
(20) Peyser, L. A.; Vinson, A. E.; Bartko, A. P.; Dickson, R. M. *Science* **2001**, *291*, 103.
(21) Peyser, L. A.; Lee, T.-H.; Dickson, R. M. *J. Phys. Chem. B* **2002**, *106*, 7725.
(22) Nepijko, S. A.; Fedorovich, R. D.; Viduta, L. V.; Ievlev, D. N.; Schulze, W. *Physica B* **2001**, *301*, 261.
(23) Nepijko, S. A.; Fedorovich, R. D.; Viduta, L. V.; Ievlev, D. N.; Schulze, W. *Ann. Phys. (Berlin)* **2000**, *9*, 125.
(24) Burke, P. J.; Spielman, I. B.; Eisenstein, J. P.; Pfeiffer, L. N.; West, K. W. *Appl. Phys. Lett.* **2000**, *76*, 745.
(25) Alameddin, G.; Hunter, J.; Cameron, D.; Kappes, M. M. *Chem. Phys. Lett.* **1992**, *192*, 122.
(26) Tjeng, L. H.; Meinders, M. B. J.; Elp, J. v.; Ghijsen, J.; Sawatzky, G. A.; Johnson, R. L. *Phys. Rev. B* **1990**, *41*, 3190.
(27) Bonacić-Koutecky, V.; Veyret, V.; Mitrić, R. *J. Chem. Phys.* **2001**, *115*, 10450.
(28) Bonacić-Koutecky, V.; Pittner, J.; Boiron, M.; Fantucci, P. *J. Chem. Phys.* **1999**, *110*, 3876.
(29) Datta, S.; Tian, W.; Hong, S.; Reifenberger, R.; Henderson, J. I.; Kubiak, C. P. *Phys. Rev. Lett.* **1997**, *79*, 2530.
(30) Pinner, D. J.; Friend, R. H.; Tessler, N. *Appl. Phys. Lett.* **2000**, *77*, 1493.
(31) Henglein, A. *J. Phys. Chem.* **1993**, *97*, 5457.
(32) Pinner, D. J.; Friend, R. H.; Tessler, N. *J. Appl. Phys.* **1999**, *86*, 5116.
(33) Huang, Y.; Duan, X. F.; Cui, Y.; Lauhon, L. J.; Kim, K. H.; Lieber, C. M. *Science* **2001**, *294*, 1313.
(34) Duan, X. F.; Huang, Y.; Lieber, C. M. *Nano Lett.* **2002**, *2*, 487.